

**Hydrodynamic-dissipation relation for characterizing flow stagnation**Seth Davidovits *Lawrence Livermore National Laboratory, Livermore, California 94550, USA*E. Kroupp , E. Stambulchik , and Y. Maron*Faculty of Physics, Weizmann Institute of Science, Rehovot 7610001, Israel* (Received 31 December 2020; revised 22 March 2021; accepted 11 May 2021; published 7 June 2021)

Hydrodynamic stagnation converts flow energy into internal energy. Here we develop a technique to directly analyze this hydrodynamic-dissipation process, which also yields a lengthscale associated with the conversion of flow energy to internal energy. We demonstrate the usefulness of this analysis for finding and comparing the hydrodynamic-stagnation dynamics of implosions theoretically, and in a test application to Z-pinch implosion data.

DOI: [10.1103/PhysRevE.103.063204](https://doi.org/10.1103/PhysRevE.103.063204)**I. INTRODUCTION**

An essential element of the implosion of a fluid or plasma is the process of stagnation, whereby the hydrodynamic energy of the implosion is converted into thermal energy. When an implosion is modeled or simulated in one dimension (the radial direction), this stagnation process proceeds ideally; at each instant in time, the momentum of the flows converging to the stagnation point is exactly balanced by an oppositely directed flow mirrored over the stagnation point (or the stagnation line in the cylindrical case). Taking the stagnation point (or line) as the origin, we have perfect rotational symmetry for the imploding flow,  $V(r, \theta, \phi, t) = V(r, t)$ , or for the cylindrical case,  $V(r, \theta, z, t) = V(r, t)$ , with no  $z$  variation as well.

When it proceeds ideally, the process of implosion and stagnation is highly effective at creating hot, high-density matter, such as in the formation of stars [1–4], or during laboratory experiments to generate fusion energy, or an intense burst of x-rays or neutrons [5–8]. In practice, implosion and stagnation rarely proceed in an ideal [one-dimensional (1D)] manner, due to a variety of possible causes, e.g., asymmetry of the implosion drive or of the initial conditions, or instabilities such as Richtmyer-Meshkov or Rayleigh-Taylor [9–21]. When the implosion process is not ideal, the perfect balance of hydrodynamic momentum at stagnation is no longer guaranteed, and residual (nonradial) momentum may be left in flows during and after the stagnation process. This momentum may still dissipate into thermal energy, but the effect of nonideal stagnation is generally a reduction in the peak density and temperature. While such a reduction is often an undesirable effect, imbalanced or unstable flow stagnation is sometimes purposefully employed to generate turbulence for study (see, e.g., Refs. [22–24]).

In plasma compression experiments, the consequences of this reduction in the achieved peak density and temperature, such as less-than-ideal (fusion) neutron or x-ray production, are often used as an implied measure of the nonideality of

the implosion. That is, comparing experimental results to 1D simulation results, and noting the difference, allows for an indirect inference of the degree to which the implosion proceeded ideally. Because of the importance of achieving an ideal implosion, a variety of diagnostics have been used to elucidate implosion symmetry (see, e.g., Refs. [15,25–28]), which, however, inform only indirectly on the hydrodynamics (flows) of stagnation.

Here, we propose a complementary technique for assessing flow stagnation that directly infers certain properties of the hydrodynamic flow at stagnation and its conversion to thermal energy. It can be applied both to assess the ideality of implosions, and also to turbulent flows, for example to infer a turbulent forcing lengthscale. Additionally, this technique uses a general starting point, which may enable it to be usable and *comparable* across differing stagnations. It requires only spatially integrated hydrodynamic information, which is often the kind of data obtainable in measurements.

Hydrodynamic stagnation is the process of dissipation of the implosion flow energy into internal and thermal energy of the compressing material. A key point of the present work is that we can compute a characteristic lengthscale for this conversion process, and this characteristic scale behaves very differently for ideal versus highly nonideal stagnations. If we consider a region of flow with total mass  $m$ , a characteristic velocity  $v$ , and a characteristic lengthscale  $l$ , then, on dimensional grounds, the dissipation of the flow kinetic energy in this region can be written

$$-\dot{E}_K = \eta m v^3 / l, \quad (1)$$

where the overdot is a time derivative, and  $\eta$  is a proportionality factor that we will explain shortly. For the characteristic velocity, take  $v^2 = 2E_K/m$ , that is, an average velocity that yields the total kinetic energy of the flow. As the flow evolves, all the quantities may be functions of time,  $\dot{E}_K(t)$ ,  $m(t)$ ,  $v(t)$ ,  $l(t)$ .

The present work has two pieces. First, in Sec. II, we show theoretically the utility of the hydrodynamic-dissipation relation, Eq. (1), for distinguishing ideal and nonideal stagnation. Second, in Sec. III, we develop a method to test this idea on data, and we apply it to a comparison of experimental data with synthetic data from a 2D simulation. Notably, this 2D simulation was carefully matched to the experimental conditions, and it gives quite similar radiation yield (the figure of merit for the experiment), but this new analysis shows distinguishable hydrodynamic behavior at stagnation.

## II. HYDRODYNAMIC DISSIPATION RELATION IN IDEAL AND NONIDEAL STAGNATION

For the case of flow stagnation ( $v \rightarrow 0$ ), we first examine the relation Eq. (1) in two opposite extremes. On the one hand, we consider a flow region that is purely turbulent, with no radial convergence at all; such a flow could develop as a result of a severely asymmetric or unstable stagnation (see, e.g., Refs. [22–24], where such stagnations are used to generate turbulence for study). On the other hand, we consider both spherical and cylindrical ideal, self-similar, radial stagnations. A variety of analytic stagnation solutions of this type exist; here we consider an isentropic (with adiabatic  $\gamma = 5/3$ ) spherical case [8] and an isothermal cylindrical case [29]. Following consideration of these cases, we consider a simple model for a flow containing a combination of ideal (self-similar) radial flow and turbulent flow.

We focus on the behavior of  $l(t)$ , which shows dramatic differences between ideal and turbulent stagnation (while  $v \rightarrow 0$  in both cases). In the ideal cases examined,  $l(t) \rightarrow 0$  as maximum compression is reached. In the turbulent case,  $l(t)$  has a tendency to grow in time (or remain a constant). This hydrodynamic scale, which can be nondimensionalized as a fraction of the plasma size,  $f_i(t) = l(t)/l_{\text{plasma}}(t)$ , may then represent a metric to determine the hydrodynamic ideality of implosions and to compare different implosions (say, cylindrical Z-pinch versus spherical implosion).

To understand  $l(t)$  [and  $\dot{E}_K$ ,  $v(t)$ ] in an ideal stagnation, we first consider a spherical, self-similar, isentropic stagnation as described by, for example, Atzeni and Meyer-ter-Vehn [8]. With  $h(t) = [1 + (t/t_0)^2]^{1/2}$  and  $\xi(r, t) = r/(R_0 h)$ , the profiles of radial flow and density are  $u(r, t) = rh/h$  and  $\rho(r, t) = \rho_0 h^{-3} [1 - \xi^2]^{3/2}$ . The stagnation radius (radius at maximum compression,  $t = 0$ ) is  $R_0$ , and the radial domain extends from 0 to  $R(t)$ , and  $R(t) = R_0 h$ .

Calculating the mass,  $m(t) = \int \rho(r, t) dV$  (constant here), and the total kinetic energy,  $E_K(t) = \int \rho(r, t) u(r, t)^2 dV/2$ , enables us to find  $v(t) = [2E_K(t)/m]^{1/2}$ . Calculating  $\dot{E}_K$ , and requiring it to equal the dimensional analysis expression, Eq. (1), we find  $f_i = l_{3D, \text{isentropic}}(t)/2R(t) = \sqrt{3/32} \eta (t/t_0)^2$ , where we have written  $l$  as a fraction of the diameter  $2R(t)$ ,  $f_i$ . Both  $l$  and  $f_i$  go to 0 as maximum compression is approached ( $t \rightarrow 0-$  in this case).

A similar result occurs for  $l(t)$  in the cylindrical, isothermal, stagnation solution utilized by Yu *et al.* [29]. Here,  $h(t)$  is the solution to the differential equation,  $\dot{h} = -\sqrt{2} \ln h/t_0$ , for times during the compression phase ( $t < 0$ ). Here,  $t_0 = \sqrt{\rho_0/\rho_0} R_0$ , with  $\rho_0$  the final (peak) pressure. We again have  $h(t = 0) = 1$ . With this  $h(t)$ ,  $u(r, t)$  and  $\xi(r, t)$  are unchanged

from the spherical case, while the density profile is  $\rho(r, t) = \rho_0 h^{-2} \exp[-\xi^2/2]$ . The domain in  $r$  now extends to  $r \rightarrow \infty$ . Carrying out the same procedure for finding  $l(t)$  as in the spherical case, we find

$$f_i = l_{2D, \text{isothermal}}(t)/2R(t) = \sqrt{2} \eta \ln h, \quad (2)$$

which also goes to 0 as maximum compression is approached ( $t \rightarrow 0-$  or  $h \rightarrow 1+$ ).

Turning now to  $l(t)$  in a turbulent flow, we discuss two studied limits. First, the simplest case is steady forced turbulence, where flow dissipation is balanced by the input flow energy, and  $E_K$  is a constant. Then  $v(t)$  and  $l(t)$  are also constants, assuming forcing at a fixed spatial scale. Furthermore,  $l(t) = l_f$  corresponds to this constant spatial forcing scale [30].

Second, we consider freely decaying turbulence (with no flow energy input). At high Reynolds numbers,  $v(t)$  and  $l(t)$  exhibit power-law behavior in time. For supersonic turbulent flows (the flows in the Z-pinch experiments considered later are supersonic or nearly so), the velocity decays as  $v(t) = v_0(1 + t/t_0)^{-\alpha/2}$ , while the lengthscale increases in time as  $l(t) = l_0(1 + t/t_0)^{\alpha/2}$ , where  $t_0 \approx l_0/v_0$  and  $\alpha \approx 1$ , albeit with some uncertainty in  $\alpha$  [30,31]. Here,  $t \geq 0$ . When the turbulence is subsonic, these power-law forms of  $v(t)$  and  $l(t)$  generally still hold at high Reynolds numbers, with the velocity decreasing and the lengthscale increasing, but with possibly somewhat different powers (see, e.g., Refs. [32–34]). One may also consider decaying turbulence with a saturated lengthscale (such as may occur in decaying wall-bounded turbulence). In this case, the  $v(t)$  decay is still a power law, but with higher  $\alpha \approx 2$  [34,35].

Simulation results in the supersonic decay case are well fit with a single value of  $\eta$  [30], motivating the assumption here that this proportionality factor is a constant; to the extent it varies in time in the general case, this time dependence will be rolled into  $l(t)$ . In this case, we have  $\eta = 2\pi \eta_v = 0.42$  [30], and we use this value of  $\eta$ . Strictly speaking, in the turbulent case, the velocity entering Eq. (1) is the root-mean-square turbulent velocity,  $v_{\text{rms}}$ , and the relation  $v^2 = 2E_K/m$  only holds approximately when  $v = v_{\text{rms}}$  because there can be modest correlations between velocity and mass fluctuations [30].

If we use the substitution  $l = f_i 2R$  and define  $y = \eta m v^3/2R$ , Eq. (1) can be written  $y = f_i \times (-\dot{E}_K)$ . The top panel of Fig. 1 shows the behavior of  $y$  versus  $x = -\dot{E}_K$  for both the cylindrical ideal solution ( $k_i = 0$ ) and a turbulent decay case ( $k_i = 10$ ). In the cylindrical stagnation case, the plot covers times just preceding peak dissipation through to stagnation; the horizontal approach of the  $k_i = 0$  curve to the origin coincides with  $f_i \rightarrow 0$  in Eq. (2) as  $t \rightarrow 0$  (and  $v \rightarrow 0$ ). In the turbulent case, peak dissipation occurs starting from the initial state. The lower panel of Fig. 1 shows  $f_i$  versus  $-\dot{E}_K$  for these same cases; we can see  $f_i \rightarrow 0$  as stagnation is approached in the ideal cylindrical stagnation, while  $f_i$  remains a significant fraction of the plasma diameter in the turbulent case.

We now discuss further the physical meaning of the lengthscale  $l$  associated, through Eq. (1), with the dissipation of hydrodynamic motion. As discussed above, for turbulence,

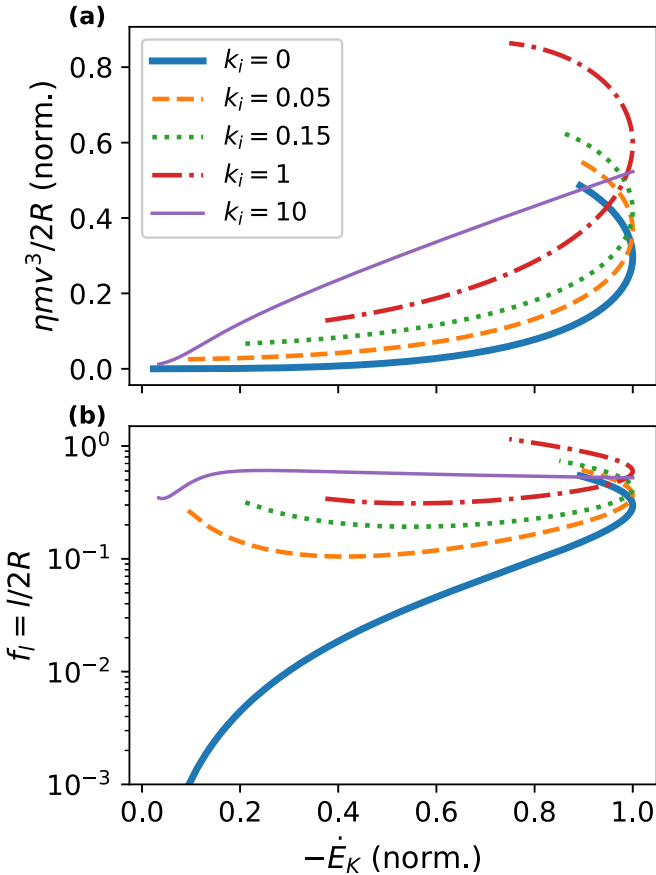


FIG. 1. (a) Inferred kinetic energy dissipation rate ( $y = \eta m v^3 / 2R$ ) at the flow scale ( $2R$ ) vs kinetic energy dissipation rate ( $x = -\dot{E}_K$ ) for a region containing different initial proportions of kinetic energy in self-similar cylindrical stagnation flow and nonstagnating (turbulent) flow. When  $k_i = 0$  (blue, thicker solid line), the region contains only the self-similar stagnation flow. When  $k_i = 10$  (purple, thinner solid line), the nonstagnating (turbulent) flow has ten times the energy of self-similar flow and dominates the dynamics; intermediate cases are also shown. Time (implicit) progresses clockwise along each curve; in the  $k_i = 10$  case, it progresses from right to left. For each case, both dissipation values are normalized to the peak  $-\dot{E}_K$ . (b) The fractional hydrodynamic (dissipation) lengthscale  $f_l$  vs the kinetic energy dissipation rate for the cases from (a); time is implicit as above. Plotted model parameters  $h_i = 2.5$ ,  $\bar{\lambda} = 0.35$ , and  $\eta = 0.42$ ; see Sec. II A.

this lengthscale corresponds in the simplest case (homogeneous, isotropic, steady forcing) with the forcing scale (spatial wavelength). Then, for turbulence forced in a narrow range of scales (wavelengths, or Fourier wave numbers),  $l$  is associated with the peak of the energy spectrum in wavelength space, i.e., roughly, the dominant wavelength of spatial variation of the flow.

In general, this characteristic wavelength of flow variation need not be associated with a corresponding spatial variation in the density. For example, in the incompressible flow limit, the density is uniform for any flow field. In the more general case, the turbulent density distribution depends on the Mach number, among other factors (see, e.g., Ref. [36]). Considering the self-similar stagnation cases discussed above, we see

that here too, the lengthscale  $l$  need not correspond with scales of density variation. At stagnation, for example, the profiles of density (and temperature in the adiabatic spherical case) vary over the stagnation radius,  $R_0$ , while  $l \rightarrow 0$ . This fact helps illustrate the complementary nature of the current approach to looking at stagnation dynamics when compared with approaches focused on the symmetry of density or temperature (or some combination of the two).

Consider some mass,  $m$ , with flow energy  $E_K$  (thereby defining  $v$ ). With these quantities fixed, a shrinking lengthscale  $l$  implies, through Eq. (1), a growing dissipation rate of the hydrodynamic motion. Evidently the “ideal” self-similar implosions considered above, with  $f_l \rightarrow 0$  ( $l \rightarrow 0$ ) as stagnation is approached, have very high dissipation rates in this metric during the period leading up to stagnation. We have already contrasted this lengthscale behavior with turbulent flow dissipation, which does not show this strong increase in relative dissipation ( $f_l$ ). As a further contrasting case, also with zero mean flow, consider a flow in solid body rotation. Since (in an idealized case) this configuration has no dissipation of the hydrodynamic energy, we have  $l \rightarrow \infty$ . Considering the spherical self-similar implosion solution discussed above at times well before stagnation, as  $t \rightarrow -\infty$ , we similarly find  $f_l \rightarrow \infty$ , corresponding again to vanishing dissipation of the finite initial kinetic energy.

Here we work in terms of  $l$  (and  $l$  normalized to the plasma size,  $f_l$ ), but we could instead work with a dissipation timescale  $\tau = l/v \sim -E_K/\dot{E}_K$ . This slightly alternate view is still an analysis based on the hydrodynamic-dissipation relation, Eq. (1). In this case, the self-similar stagnation solutions have  $\tau \rightarrow 0$  as stagnation is approached, i.e., an increasingly short dissipation timescale. For the steadily forced or decaying supersonic turbulence cases discussed above,  $\tau$  will be, respectively, constant or growing in time.

### A. Basic model for mixed stagnation

Figure 1 also shows cases that are intermediate between the pure cylindrical self-similar stagnation solution and a turbulence-dominated case. All cases are labeled by  $k_i = E_{T,i}/E_{S,i}$ , which is the initial ratio of turbulent kinetic energy,  $E_T$ , to cylindrical stagnation solution kinetic energy,  $E_S$ . Here, the plasma starts with this initial energy mix at some radius (taken as  $h_i = 2.5$ ,  $R_i = h_i R_0$ , in Fig. 1) and then evolves in time in a manner we now describe.

To get a more general sense for  $f_l$  and the hydrodynamic-dissipation relation, Eq. (1), we consider an essentially heuristic treatment for a mass of plasma containing a mix of stagnating flow and some nonstagnating flow (statistically uncorrelated with the radial stagnation flow). We treat this nonstagnating flow as turbulent for the sake of calculating its dissipation; this is discussed further at the end of the present section. For this mixed-flow plasma, we treat the stagnating flow identically to the self-similar cases discussed above, here using the isothermal cylindrical solution. In other words, the stagnating flow component is treated as unaffected by the presence of the statistically uncorrelated nonstagnating flow.

Then this component’s flow quantities follow as above, and in particular we have the stagnating flow kinetic energy,  $E_S = M v_S^2 / 2$ , with  $M$  the constant total mass,

and  $v_S = 2(R_0/t_0)\sqrt{\ln h}$  is the average velocity characterizing the total kinetic energy. We similarly write the turbulent-component kinetic energy  $E_T = Mv_T^2/2$ . Thus  $k_i = (v_{T,i}/v_{S,i})^2$ .

The characteristic turbulent velocity,  $v_T$ , evolves according to

$$\frac{d(v_T^2/2)}{dt} = -\frac{2\dot{h}}{3h}v_T^2 - \frac{\eta}{\bar{\lambda}}\frac{v_T^3}{2R_0h}. \quad (3)$$

This model equation is based on existing models [37,38] of turbulence undergoing compression in velocity fields that are linear in radius [ $u(r,t) \sim r$ ], as is the case here. The first term on the right-hand side of Eq. (3) models energy injection into the turbulence by the compression (two-dimensional compression in this case, with no compression along  $z$ ). The second term models the turbulent dissipation in the high-Reynolds-number limit for a flow with a saturated lengthscale [30,39].

This lengthscale is taken as a fraction of the (changing) plasma diameter  $l = \bar{\lambda}2R_0h$ . By saturated lengthscale, we refer to the use of a constant value of  $\bar{\lambda}$  (constant fraction of the plasma size). Then, in the pure turbulent decay case  $\dot{h} = 0$ ,  $v_S = 0$ , we will find  $f_l = \bar{\lambda}$ . We use this saturated lengthscale form of the dissipation here partly for convenience in solving the model, and also because there are existing computed values for  $\bar{\lambda}$  for compressing turbulence, with prior work finding  $\bar{\lambda} \sim 0.19$  in a low-Mach case [38,40] (the forcing studied in Ref. [40] mimics compression) and  $\bar{\lambda} \sim 0.35$  in a supersonic isothermal turbulence case [37]. The plots in Fig. 1 use  $\bar{\lambda} = 0.35$ .

Equation (3) can be solved explicitly for  $v_T$ , with an initial condition  $v_{T,i} = v_T(h = h_i)$  that can be expressed in terms of  $v_S$  and  $k_i$ . Defining the total kinetic energy  $E = E_T + E_S$  and the (total) characteristic velocity  $v = \sqrt{2E/M}$ , we can again compute the components of the dissipation relation, Eq. (1), and the (combined) hydrodynamic-dissipation lengthscale. Defining  $\bar{v}_T = v_T/(R_0/t_0)$  and explicitly writing  $f_l = l/2R$  and  $\bar{v}_T$ , we have

$$f_l = \frac{\eta}{4\sqrt{2\ln h}}(4\ln h + \bar{v}_T^2)^{3/2} \left(1 - \frac{\bar{v}_T^2}{3} + \frac{\eta\bar{v}_T^3}{\bar{\lambda}4\sqrt{2\ln h}}\right)^{-1}, \quad (4)$$

$$\bar{v}_T = \frac{2}{h^{2/3}} \left\{ \frac{1}{h_i^{2/3}\sqrt{k_i \ln h_i}} + \sqrt{\frac{3\pi}{4}} \frac{\eta}{\bar{\lambda}} [E(h_i) - E(h)] \right\}^{-1}. \quad (5)$$

Here we use the shorthand  $E(h) \equiv \text{Erf}[\sqrt{2\ln h/3}]$ .

In writing the model equation for  $v_T$ , Eq. (3), we have assumed that this turbulent component is isotropic. The assumed value of  $\bar{\lambda}$  also comes from simulations in which the compression (and turbulent energy) is isotropic. Since the compressions at hand are cylindrical, this means there is an assumption either that the turbulent energy is generated isotropically or that nonlinear interactions are sufficient to isotropize it (on the one hand, in turbulence driven by large two-dimensional compression this need not be the case [41]; on the other hand, turbulence experiments often generate turbulence by colliding flows in planar geometry [22–24]).

Practically, if we alter this isotropy assumption, we should still expect distinguishable behavior between  $k_i = 0$  and  $k_i \neq$

0 in Fig. 1. Further, since here we take  $h_i = 2.5$ , the effects of compression on the turbulent component in Fig. 1 are already quite modest; most important is that for  $k_i \neq 0$  we now have two hydrodynamic components that dissipate differently.

Note that the stagnating flow *completely* converts (dissipates) its kinetic energy in the time  $t_i = t_0\sqrt{\pi/2}\text{Erfi}(\sqrt{\ln h_i})$ , which is on order of  $t_0$  for  $h_i$  not too large. We may write an initial turbulent dissipation timescale as  $\tau_{T,i} = l_i/v_{T,i} = t_0(\bar{\lambda}h_i)/(\sqrt{k_i \ln h_i})$ . This will again be on order of  $t_0$  for a range of  $h_i, k_i, \bar{\lambda}$ ; however, this dissipation timescale is now in the sense of a power-law decay rather than complete conversion. Thus, in the finite time to stagnation ( $h = 1$ ), there can be incomplete dissipation of  $E_T$ ; this leads to certain curves in Fig. 1 ending far from 0,0 when plotted on the interval  $h \in [h_i, 1]$ . The  $k_i = 10$  curve, having a shorter dissipation timescale, dissipates more substantially over the interval, but its behavior is still distinct from the ideal stagnation because the *lengthscale* associated with this dissipation is very different.

This turbulent dissipation timescale is still fast in many cases compared to other ways in which we may consider that nonstagnating flow dissipates (e.g., the viscous decay timescale is longer by on order of the Reynolds number). Other dissipation mechanisms may have different lengthscale behaviors. In general, we may expect that substantial changes in the  $y$  versus  $-\dot{E}_K$  and  $f_l$  curves can still occur for  $E_T$  dissipating in a manner other than turbulent dissipation, when the dissipation mechanism is not matched in rate and lengthscale to the stagnation energy conversion.

### III. DEMONSTRATION APPLICATION

We seek to produce the curve  $y$  versus  $-\dot{E}_K$  during a stagnation and to infer  $l(t)$ . To do so requires measurements of  $\dot{E}_K$ ,  $m$ , and  $v$ . Here we work with experimental measurements from the stagnation period of gas-puff Z-pinch [10,19], and synthetic data from 2D simulations designed to match the experiments [42]. These data consist of a set of radiation measurements of the stagnating plasma, which are discussed in more detail elsewhere [10,19,43]; we treat synthetic and experimental data the same. Both the experiments and the matching simulations focused on analyzing only a subset ( $L_{\text{pl}} = 2$  mm) of the  $z$  extent of the stagnating plasma, which was observed to have peak radiation emission at a similar time (the exact stagnation time varies along the column). Then, we expect that the 2D ( $r, z$ ) simulations will stagnate approximately ideally, lacking any  $\theta$  variation, while the experiments may have such variation. First we describe the time-dependent inference of  $m$  and  $v$ , then we discuss the estimation of  $-\dot{E}_K$ .

The Z-pinch experimental measurements (Table I of Ref. [19]) give, at six times during stagnation, the plasma radius  $r_{\text{pl}}$ , electron density  $n_e$ , and an inference of the plasma kinetic energy through measurements of the total Doppler-broadened ion energy and the electron temperature. Together these permit us to calculate the radiating plasma volume and  $m(t)$  and  $v(t)$  for the six measurement times.

We calculate  $l_{\text{pl}}(t) = 2r_{\text{pl}}^{\text{turb}}$ ,  $v(t) = [3k(T_i^{\text{eff}} - T_i)/m_i]^{1/2}$ , and  $m(t) = (n_e^{\text{turb}}/\bar{Z})m_iV_{\text{pl}}$ , with the plasma volume  $V_{\text{pl}}(t) = \pi(r_{\text{pl}}^{\text{turb}})^2L_{\text{pl}}$  and  $\bar{Z} \approx 8$ . Here  $T_i^{\text{eff}}$  is a total Doppler-broadened

ion temperature,  $T_i$  is the thermal ion temperature, and  $n_e^{\text{turb}}$  is an electron density inferred through a combination of radiation measurements. We use the radiating plasma diameter,  $l_{\text{pl}}(t)$ , which is measured through x-ray pinhole imaging at the six times as the reference lengthscale,  $f_l = l/l_{\text{pl}}$ .

Possessing measurements of  $m(t)$  and  $v(t)$ , we could directly calculate  $\dot{E}_K \approx \Delta(mv^2/2)/\Delta t$  by taking the approximate time derivative using our data. It is important to note that we are looking for time variation of  $E_K$  in Eq. (1) that has to do with *dissipation* of hydrodynamic motion, rather than changes in hydrodynamic motion, say, due to flows into or out of the measurement region. Given the type of observations available for the current experiments, we do not pursue this direct derivative strategy to try to reduce the influence on our measurements of unknown flows of hydrodynamic energy into or out of the measurement region.

Instead, we proceed as follows. At present, we infer the radiating mass and  $v_{\text{rms}}$  at six times in the hottest, densest, part of the stagnation using  $K$ -shell radiation measurements [10,19]. When hydrodynamic motion is dissipated in this region, it flows into ion and electron thermal energy, which are equilibrated on a timescale that is very fast compared to the stagnation time [10]. Some portion of this energy is then radiated; if this radiation is considered to be time-local to the hydrodynamic dissipation, then we write

$$-\dot{E}_K = P_R + \dot{E}_O = P_R(1 + \dot{E}_O/P_R), \quad (6)$$

with  $P_R$  the radiated power, which is measured at each time. Here  $\dot{E}_O$  is other changes in the plasma energy, at present principally changes in plasma thermal and internal energies. This approach is motivated by the observation that, over the whole of the stagnation time period, the total radiation can be accounted for by changes in the hydrodynamic motion [10,43], a fact first noted in other Z-pinch experiments [44].

While the timescale for collisional-radiative equilibrium is shorter than the stagnation period, it is not necessarily a well-separated timescale, so that time-locality of the radiation to the hydrodynamic dissipation is only approximate. Nonetheless, by pursuing this strategy for inferring  $\dot{E}_K$ , we infer  $m$ ,  $v_{\text{rms}}$ , and  $P_R$  (representing a portion of  $\dot{E}_K$ ) using *the same plasma and radiative state*. Together with Eq. (1), Eq. (6) gives a relation for  $f_l = l/l_{\text{pl}}$ ,

$$\eta mv^3/l_{\text{pl}} = f_l P_R(1 + \dot{E}_O/P_R). \quad (7)$$

Panels (a) and (b) in Fig. 2 show a plot of  $y = \eta mv^3/l_{\text{pl}}$  against  $P_R$  for the experimental and synthetic (simulation) data, respectively. To estimate  $P_R$  from the absolutely calibrated hard-x-ray measurements ( $P_{\text{PCD}}$  in Table I of Ref. [19]), we write  $P_R = P_{\text{PCD}}[1 + \Delta(T_e)]$ , where  $\Delta$  is a temperature-dependent factor calculated using a collisional-radiative code, which estimates the ratio of soft radiation to that picked up in the hard-x-ray measurements. For all but the first and last times,  $\Delta \lesssim 30\%$ ; the analysis can also be carried out using the raw  $P_{\text{PCD}}$  without changing the essence.

When  $l$  is small in Eq. (1), a small change in  $\eta mv^3$  ( $\sim y$ ) leads to a large change in  $-\dot{E}_K$ . For the  $k_i = 0$  case in the top plot of Fig. 1, this fact corresponds with the horizontal approach of the curve  $y(t)$ ,  $-\dot{E}_K(t)$  to the origin as ideal stagnation is approached and  $f_l \rightarrow 0$ . Similar behavior (though

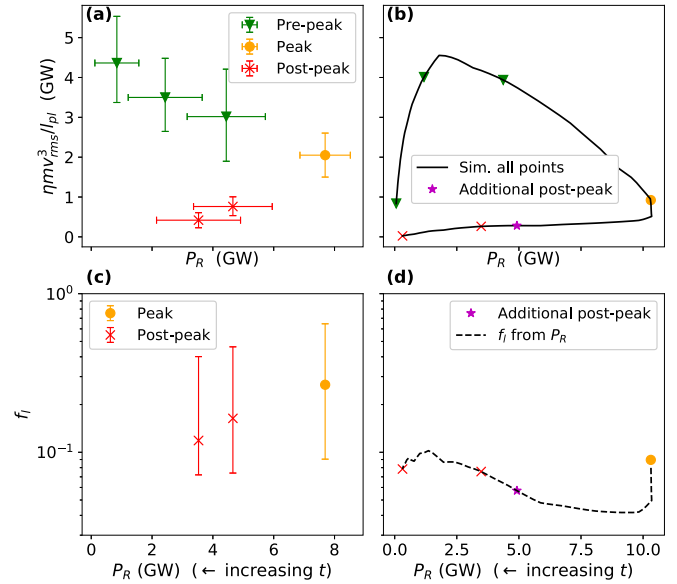


FIG. 2. (a),(b) Scatter plots of  $y$  vs  $P_R$  for Z-pinch experiment data and synthetic data from matched 2D simulations, respectively. On the right, the continuous simulation data are shown (black, solid) in addition to simulation points matched in time to the experimental measurements (plus one “additional” data point because the last matched time is  $P_R \sim 0$  for the simulations). In both cases, time progresses clockwise from the leftmost (green) triangle. (c),(d) Instantaneous values of the fractional hydrodynamic lengthscale,  $f_l$ , inferred taking  $-\dot{E}_K \approx P_R$  for the experiments and simulations, respectively, after peak emission as stagnation is approached.

using  $P_R$ ) appears to occur in the simulation curve in Fig. 2, suggesting a small lengthscale during these times, but this behavior is not observed in the experiment. We turn now to a quantitative inference of  $f_l$ , but we raise this observation because ultimately, if we consider a larger class of stagnations than the few cases examined here, we may find the shape of the  $y$  versus  $-\dot{E}_K$  curve more easily interpreted than a specific focus on  $f_l$  [45].

The simplest approach to a quantitative estimate of  $f_l$  is to approximate  $-\dot{E}_K \approx P_R$ , allowing us to evaluate  $f_l$  at each time from measurements of  $m$ ,  $v$ , and  $P_R$  (and  $l_{\text{pl}}$ ), and this is what we do here. We note that the quantities needed for the hydrodynamic-dissipation relation technique that we outline in the present work could be generally inferred in different ways, depending on the observed system and available types of measurements.

When inferring  $f_l$  leading up to stagnation, we utilize data points after peak radiation. In the ideal solutions, flow stagnation occurs after peak dissipation ( $R_{\text{peak}} = \sqrt{e}R_0$  for the cylindrical case). For experiments with large thermal energy losses like the present ones, we may expect a shift in maximum radiation away from peak compression and toward peak  $-\dot{E}_K$ . Indeed, examining the radial velocity profiles for the simulations (Fig. 8 in Ref. [42]), we find the pinch is still compressing well after peak radiation (at +2 ns).

Plots (c) and (d) in Fig. 2 show  $f_l$ , inferred approximating  $-\dot{E}_K \approx P_R$ , from peak emission onward for the experiments and simulations. The accuracy of this inferred  $f_l$  depends on the degree to which  $\dot{E}_O/P_R$  is a correction factor; estimating

$\dot{E}_O$ , directly from the data (which also include temperature in this case), we estimate  $\dot{E}_O/P_R \sim 1/2-1/3$  for the experimental data at and after the peak emission. In both the experiment and simulations, we expect that  $f_i$  inferred this way is more accurate nearer to peak radiation (e.g., for  $P_R \gtrsim 5$  GW). While the instantaneous  $f_i$ , inferred using  $P_R$ , will not be exact because  $P_R$  represents only a portion of  $\dot{E}_K$ , it may be sufficient for a relative measure of stagnation ideality between similar experiments where the energy flow dynamics are in comparable regimes. In principle, one could create models for the apportionment of  $\dot{E}_K$  in Eq. (6).

The instantaneous  $f_i$  for the experiment are generally in the 0.1–0.3 range ( $\sim 0.12$  to  $\sim 0.27$ ), indicating a hydrodynamic lengthscale that is 10–30 % of the radiation diameter, or a lengthscale of roughly 80–240  $\mu\text{m}$ . The available temperature measurements [19] suggest  $\dot{E}_O < 0$ , so that  $f_i$  from the instantaneous analysis may be an underestimate.

These  $f_i$  are generally consistent with  $\bar{\lambda} \sim 0.19$ , 0.35 from the (homogeneous, isotropic) compressing turbulence simulation cases mentioned in Sec. II A. We should be cautious applying this intuition in isolation, since in principle  $f_i$  could take such values for other reasons as well. In the ideal self-similar solution,  $f_i \sim 0.03$  by the time  $-\dot{E}_K$  is half its peak value in Fig. 1, but we can see that even modest amounts of  $k_i \neq 0$  give  $f_i \gtrsim 0.1$  with the chosen set of model parameters. It is important to note that the profiles of the hydrodynamic quantities in the present experiments need not (and probably do not) match the self-similar profiles of the basic model.

The firmer theoretical comparison is the result from the detailed simulation, shown in panel (d) of Fig. 2. We see that, at peak  $P_R$ ,  $f_i$  is smaller in the simulation data than in the experimental data; this behavior is consistent with the behavior for smaller (or zero)  $k_i$  in the model Fig. 1. Further, the simulation generally shows smaller values of  $f_i$  in the region of high  $P_R$  where this  $f_i$  is likely a better estimate, indicating hydrodynamic dissipation at a smaller scale, which is therefore more consistent with ideal stagnation. We see  $f_i \approx 0.04$  at  $P_R \sim 6-8$  GW, yielding  $l \approx 35$   $\mu\text{m}$  for a minimum hydrodynamic scale ( $l_{\text{pl}} \approx 880$   $\mu\text{m}$ ), while the experimental  $f_i$  and  $l$  are nearly an order of magnitude larger at comparable  $P_R$  after peak emission.

Note that we may find that  $f_i$  evaluated exactly from the simulations underlying the simulated data presently used does not decrease all the way to 0, both because there is still some small averaging in  $z$  over plasma that may stagnate at slightly different times, and because the radial flow solution is not the self-similar one (perhaps in particular, the flow does not momentarily go to 0 everywhere at stagnation as in the ideal self similar case).

In calculating the experimental quantities in Fig. 2, we have used a plasma radius and density inferred (in Ref. [19]) using an analysis that accounts for the likely nonuniform density in the radiating plasma and is therefore more complex than an analysis assuming a uniform radiating plasma. However, we note that the results in Fig. 2 are not so sensitive to these assumptions, and in particular, the analysis repeated assuming a uniform plasma yields nearly identical values for  $f_i$  (the uniform plasma data are also summarized in Ref. [19]). Similarly, the plasma kinetic energy in the present data is inferred, in

part, using energy balance arguments [10], but similar results have been found in additional experiments using a completely independent technique (see Ref. [20] and Fig. 8 and the surrounding discussion in Ref. [46]).

In any event, we hope that the present demonstration application is useful independent of the details of this particular Z-pinch case. We have highlighted a number of practical considerations in inferring the hydrodynamic-dissipation relation quantities in a plasma, such as the distinction between changes in  $E_K$  due to dissipation versus flows into or out of the observed plasma. Additionally, we raised and explored the possibility of using  $P_R$  as a surrogate for  $-\dot{E}_K$ , and, although the quantity of data is limited, we found that  $f_i$  inferred in this way apparently distinguishes a closely matched 2D simulation from its experiment counterparts.

#### IV. SUMMARY

In summary, here we have developed a technique for directly inferring properties of the conversion of flow energy to internal energy in stagnation. We have demonstrated the utility of this technique for assessing the turbulent dissipation scale as well as the ideality (hydrodynamic symmetry) of implosions through the use of a lengthscale fraction  $f_i$ . We show that  $f_i \rightarrow 0$  with an approach to stagnation in two theoretical ideal compression cases, one spherical and one cylindrical, while it tends to grow or remain steady for turbulence. We also show the behavior of  $f_i$  and the hydrodynamic-dissipation curve  $y = \eta m v^3 / l$  versus  $-\dot{E}_K$  in a basic model for a flow region containing a mix of stagnating and nonstagnating (turbulent) flow.

A powerful aspect of the present technique is that it essentially infers spatial information about flows, without requiring any spatial resolution of them. This may make the technique particularly useful for those experiments in which spatially resolving features of the flows is difficult or infeasible. Because of the generality of the framework, we hope that the technique shown here enables a variety of implosions or flow stagnations to be assessed and generates new insights into this important process.

#### ACKNOWLEDGMENTS

The authors would like to acknowledge the Princeton-Weizmann-CNRS-HIT Plasma Workshop held at the Weizmann Institute for helping to spur the work, and to thank J. L. Giuliani for providing the simulation plot data from Ref. [42]. S.D. performed his work under the auspices of the US Department of Energy by Lawrence Livermore National Laboratory under Contract No. DE-AC52-07NA27344 and was supported by the LLNL-LDRD Program under Project No. 20-ERD-058. The work of E.K., E.S., and Y.M. was supported by BSF-NSF (USA) and BSF (US-Israel Binational Science Foundation).

This document was prepared as an account of work sponsored by an agency of the United States government. Neither the United States government nor Lawrence Livermore National Security, LLC, nor any of their employees makes any warranty, expressed or implied, or assumes any legal liability or responsibility for the accuracy, completeness, or usefulness

of any information, apparatus, product, or process disclosed, or represents that its use would not infringe privately owned rights. Reference herein to any specific commercial product, process, or service by trade name, trademark, manufacturer, or otherwise does not necessarily constitute or imply its endorsement, recommendation, or favoring by the United States

government or Lawrence Livermore National Security, LLC. The views and opinions of the authors expressed herein do not necessarily state or reflect those of the United States government or Lawrence Livermore National Security, LLC, and shall not be used for advertising or product endorsement purposes.

- [1] R. B. Larson, *Mon. Not. R. Astron. Soc.* **145**, 271 (1969).
- [2] M. V. Penston, *Mon. Not. R. Astron. Soc.* **144**, 425 (1969).
- [3] A. Whitworth and D. Summers, *Mon. Not. R. Astron. Soc.* **214**, 1 (1985).
- [4] Y.-Q. Lou and C.-H. Shi, *Mon. Not. R. Astron. Soc.* **442**, 741 (2014).
- [5] J. Nuckolls, L. Wood, A. Thiessen, and G. Zimmerman, *Nature (London)* **239**, 139 (1972).
- [6] J. Lindl, *Phys. Plasmas* **2**, 3933 (1995).
- [7] D. D. Ryutov, M. S. Derzon, and M. K. Matzen, *Rev. Mod. Phys.* **72**, 167 (2000).
- [8] S. Atzeni and J. Meyer-ter-Vehn, *The Physics of Inertial Fusion: Beam Plasma Interaction, Hydrodynamics, Hot Dense Matter* (Oxford University Press, Oxford, 2004).
- [9] E. I. Moses, R. N. Boyd, B. A. Remington, C. J. Keane, and R. Al-Ayat, *Phys. Plasmas* **16**, 041006 (2009).
- [10] E. Kroupp, D. Osin, A. Starobinets, V. Fisher, V. Bernshtam, L. Weingarten, Y. Maron, I. Uschmann, E. Förster, A. Fisher, M. E. Cuneo, C. Deeney, and J. L. Giuliani, *Phys. Rev. Lett.* **107**, 105001 (2011).
- [11] T. J. Awe, R. D. McBride, C. A. Jennings, D. C. Lamppa, M. R. Martin, D. C. Rovang, S. A. Slutz, M. E. Cuneo, A. C. Owen, D. B. Sinars, K. Tomlinson, M. R. Gomez, S. B. Hansen, M. C. Herrmann, J. L. McKenney, C. Nakhleh, G. K. Robertson, G. A. Rochau, M. E. Savage, D. G. Schroen *et al.*, *Phys. Rev. Lett.* **111**, 235005 (2013).
- [12] R. H. H. Scott, D. S. Clark, D. K. Bradley, D. A. Callahan, M. J. Edwards, S. W. Haan, O. S. Jones, B. K. Spears, M. M. Marinak, R. P. J. Town, P. A. Norreys, and L. J. Suter, *Phys. Rev. Lett.* **110**, 075001 (2013).
- [13] D. S. Clark, M. M. Marinak, C. R. Weber, D. C. Eder, S. W. Haan, B. A. Hammel, D. E. Hinkel, O. S. Jones, J. L. Milovich, P. K. Patel, H. F. Robey, J. D. Salmonson, S. M. Sepke, and C. A. Thomas, *Phys. Plasmas* **22**, 022703 (2015).
- [14] C. R. Weber, D. S. Clark, A. W. Cook, D. C. Eder, S. W. Haan, B. A. Hammel, D. E. Hinkel, O. S. Jones, M. M. Marinak, J. L. Milovich, P. K. Patel, H. F. Robey, J. D. Salmonson, S. M. Sepke, and C. A. Thomas, *Phys. Plasmas* **22**, 032702 (2015).
- [15] A. B. Zylstra, J. A. Frenje, F. H. Séguin, J. R. Rygg, A. Kritcher, M. J. Rosenberg, H. G. Rinderknecht, D. G. Hicks, S. Friedrich, R. Bionta, N. B. Meezan, R. Olson, J. Atherton, M. Barrios, P. Bell, R. Benedetti, L. Berzak Hopkins, R. Betti, D. Bradley, D. Callahan *et al.*, *Phys. Plasmas* **22**, 056301 (2015).
- [16] R. Betti and O. Hurricane, *Nat. Phys.* **12**, 435 (2016).
- [17] J. E. Ralph, O. Landen, L. Divol, A. Pak, T. Ma, D. A. Callahan, A. L. Kritcher, T. Döppner, D. E. Hinkel, C. Jarrott, J. D. Moody, B. B. Pollock, O. Hurricane, and M. J. Edwards, *Phys. Plasmas* **25**, 082701 (2018).
- [18] L. C. Jarrott, B. Bachmann, T. Ma, L. R. Benedetti, F. E. Field, E. P. Hartouni, R. Hatarik, N. Izumi, S. F. Khan, O. L. Landen, S. R. Nagel, R. Nora, A. Pak, J. L. Peterson, M. B. Schneider, P. T. Springer, and P. K. Patel, *Phys. Rev. Lett.* **121**, 085001 (2018).
- [19] E. Kroupp, E. Stambulchik, A. Starobinets, D. Osin, V. I. Fisher, D. Alumot, Y. Maron, S. Davidovits, N. J. Fisch, and A. Fruchtman, *Phys. Rev. E* **97**, 013202 (2018).
- [20] D. Alumot, E. Kroupp, E. Stambulchik, A. Starobinets, I. Uschmann, and Y. Maron, *Phys. Rev. Lett.* **122**, 095001 (2019).
- [21] H. G. Rinderknecht, D. T. Casey, R. Hatarik, R. M. Bionta, B. J. MacGowan, P. Patel, O. L. Landen, E. P. Hartouni, and O. A. Hurricane, *Phys. Rev. Lett.* **124**, 145002 (2020).
- [22] J. Meinecke, P. Tzeferacos, A. Bell, R. Bingham, R. Clarke, E. Churazov, R. Crowston, H. Doyle, R. P. Drake, R. Heathcote *et al.*, *Proc. Natl. Acad. Sci. USA* **112**, 8211 (2015).
- [23] P. Tzeferacos, A. Rigby, A. Bott, A. Bell, R. Bingham, A. Casner, F. Cattaneo, E. Churazov, J. Emig, F. Fiuza *et al.*, *Nat. Commun.* **9**, 591 (2018).
- [24] T. White, M. Oliver, P. Mabey, M. Kühn-Kauffeldt, A. Bott, L. Döhl, A. Bell, R. Bingham, R. Clarke, J. Foster *et al.*, *Nat. Commun.* **10**, 1 (2019).
- [25] R. P. J. Town, D. K. Bradley, A. Kritcher, O. S. Jones, J. R. Rygg, R. Tommasini, M. Barrios, L. R. Benedetti, L. F. Berzak Hopkins, P. M. Celliers, T. Döppner, E. L. Dewald, D. C. Eder, J. E. Field, S. M. Glenn, N. Izumi, S. W. Haan, S. F. Khan, J. L. Kline, G. A. Kyrala *et al.*, *Phys. Plasmas* **21**, 056313 (2014).
- [26] J. R. Rygg, O. S. Jones, J. E. Field, M. A. Barrios, L. R. Benedetti, G. W. Collins, D. C. Eder, M. J. Edwards, J. L. Kline, J. J. Kroll, O. L. Landen, T. Ma, A. Pak, J. L. Peterson, K. Raman, R. P. J. Town, and D. K. Bradley, *Phys. Rev. Lett.* **112**, 195001 (2014).
- [27] R. Tommasini, J. E. Field, B. A. Hammel, O. L. Landen, S. W. Haan, C. Aracne-Ruddle, L. R. Benedetti, D. K. Bradley, D. A. Callahan, E. L. Dewald, T. Döppner, M. J. Edwards, O. A. Hurricane, N. Izumi, O. A. Jones, T. Ma, N. B. Meezan, S. R. Nagel, J. R. Rygg, K. S. Segraves *et al.*, *Phys. Plasmas* **22**, 056315 (2015).
- [28] M. Gatu Johnson, B. D. Appelbe, J. P. Chittenden, J. Delettrez, C. Forrest, J. A. Frenje, V. Y. Glebov, W. Grimble, B. M. Haines, I. Igumenshchev, R. Janezic, J. P. Knauer, B. Lahmann, F. J. Marshall, T. Michel, F. H. Séguin, C. Stoeckl, C. Walsh, A. B. Zylstra, and R. D. Petrasso, *Phys. Rev. E* **98**, 051201(R) (2018).
- [29] E. P. Yu, A. L. Velikovich, and Y. Maron, *Phys. Plasmas* **21**, 082703 (2014).
- [30] M.-M. Mac Low, *Astrophys. J.* **524**, 169 (1999).
- [31] M.-M. Mac Low, R. S. Klessen, A. Burkert, and M. D. Smith, *Phys. Rev. Lett.* **80**, 2754 (1998).
- [32] P. Sagaut and C. Cambon, *Homogeneous Turbulence Dynamics* (Cambridge University Press, New York, 2008).
- [33] M. Sinhuber, E. Bodenschatz, and G. P. Bewley, *Phys. Rev. Lett.* **114**, 034501 (2015).
- [34] B. Thorber, *Phys. Fluids* **28**, 045106 (2016).

- [35] L. Skrbek and S. R. Stalp, *Phys. Fluids* **12**, 1997 (2000).
- [36] J. Kim and D. Ryu, *Astrophys. J.* **630**, L45 (2005).
- [37] B. Robertson and P. Goldreich, *Astrophys. J. Lett.* **750**, L31 (2012).
- [38] S. Davidovits and N. J. Fisch, *Phys. Plasmas* **24**, 122311 (2017).
- [39] D. Lohse, *Phys. Rev. Lett.* **73**, 3223 (1994).
- [40] C. Rosales and C. Meneveau, *Phys. Fluids* **17**, 095106 (2005).
- [41] S. Davidovits and N. J. Fisch, *Phys. Rev. E* **102**, 053213 (2020).
- [42] J. L. Giuliani, J. W. Thornhill, E. Kroupp, D. Osin, Y. Maron, A. Dasgupta, J. P. Apruzese, A. L. Velikovich, Y. K. Chong, A. Starobinets, V. Fisher, Y. Zarnitsky, V. Bernshtam, A. Fisher, T. A. Mehlhorn, and C. Deeney, *Phys. Plasmas* **21**, 031209 (2014).
- [43] Y. Maron, A. Starobinets, V. I. Fisher, E. Kroupp, D. Osin, A. Fisher, C. Deeney, C. A. Coverdale, P. D. Lepell, E. P. Yu, C. Jennings, M. E. Cuneo, M. C. Herrmann, J. L. Porter, T. A. Mehlhorn, and J. P. Apruzese, *Phys. Rev. Lett.* **111**, 035001 (2013).
- [44] E. Kroupp, D. Osin, A. Starobinets, V. Fisher, V. Bernshtam, Y. Maron, I. Uschmann, E. Förster, A. Fisher, and C. Deeney, *Phys. Rev. Lett.* **98**, 115001 (2007).
- [45] Consider, for example, if we added a small mean flow to the ideal cylindrical solution, which does not contribute to dissipation; this would lead to infinite  $f_i$  at “stagnation” but would give simply a vertical shift to the curve  $y$  versus  $-\dot{E}_K$ . Note that in the present experimental measurements, there is no mean flow in the inferred velocity, and it may generally be sensible to remove such a component when it enters.
- [46] Y. Maron, *Phys. Plasmas* **27**, 060901 (2020).